Membrane structure and interactions of human catestatin by multidimensional solution and solid-state NMR spectroscopy

Masae Sugawara, Jarbas M Resende, Cléria Mendonça Moraes, Arnaud Marquette, Jean-François Chich, Marie-hélène Metz-boutigue, Burkhard Bechinger

The FASEB Journal

Copy of e-mail Notification z387752

Your article (# 09-142554) from The FASEB Journal is available for downloading.

_____

The FASEB Journal is published by the Federation of American Societies for Experimental Biology (FASEB)

Dear author,
Please click on this URL address http://rapidproof.cadmus.com/RapidProof/retrieval/index.jsp then
Login: your e-mail address

Password: 4xEFVsCV5THA (You may copy and paste this case-sensitive password.)

The site contains one (1) file. You will need to have Adobe Acrobat(r) Reader software to read it. This software is freely available for download at www.adobe.com.

Please print the PDF file of your proof and read it carefully. Indicate changes or corrections in the margin of the page. If you need to provide the editorial office with a revised figure, please draw and "X" through the incorrect figure and write "NEW FIGURE FILE REQUIRED" in the margin. The compositor will contact the corresponding author to obtain the file(s).

Within 48 hours after receiving this message, please fax forms to the following fax numbers:

Fax PROOF CORRECTIONS to: 1-717-738-9479
Proof corrections sent by any other means or faxed to any other number may result in substantial publication delays.

Fax PUBLICATION FORMS to: 1-301-634-7809
Publication forms sent by any other means or faxed to any other number may result in substantial publication delays.

NOTE: Proofs or publication forms retained by the author for an excessive length of time may not be published online in a timely way and may need to be scheduled for a later print issue.

If you have any problems or questions, please contact me. Always include your article number in all correspondence.

Sincerely,
Mary Kiorpes Hayden
FASEB Office of Publications
9650 Rockville Pike
Bethesda, MD 20814-3998
phone: 301-634-7151
fax: 301-634-7809
mhayden@faseb.org

The FASEB Journal

The Journal of the Federation of American Societies for Experimental Biology

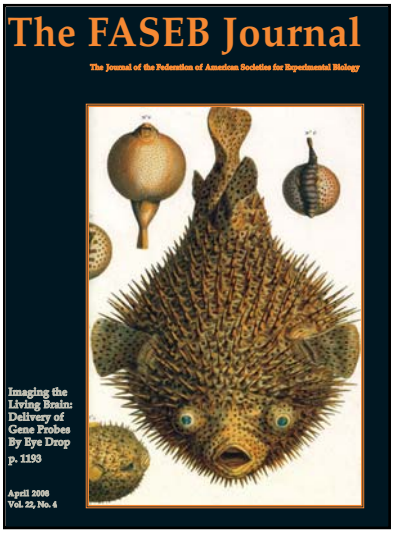

As an engaged—and engaging—source for insights into new science, *The FASEB Journal* publishes the best of peer-reviewed work in experimental biology from around the world.

As disciplines in the life sciences continue to overlap, readers are drawn to *The FASEB Journal* for its interdisciplinary coverage and perspective. *The FASEB Journal* has become a preferred venue for the latest research reports and reviews of epigenetics, iRNA mechanics, histone acetylation, nitric oxide signaling, eicosanoid biochemistry, angiogenesis, tumor suppressor genes, apoptosis, cytoskeletal function, human stem cell research, and more!

The FASEB Journal is a journal of all the Life Sciences and the Life of Science.

Join us at www.fasebj.org.

2009 Subscription Prices

	United States	Canada/ Mexico	Rest of World*
FASEB Member Print & Online	$119	$146	$227
FASEB Member Online Only	$70	$70	$70
Individual Print & Online	$225	$252	$338
Individual Online Only	$176	$176	$176
Student Online Only♦	$45	$45	$45
Institution Print & Online	$932	$960	$1045
Institution Online Only	$866	$866	$866

* includes expedited airmail, ♦ Evidence of student status required. Students wanting print and online pay Member rates.

Payment Options—Please circle desired subscription type in price chart above.

☐ VISA (13 or 16 Digits) ☐ MasterCard (16 Digits) ☐ EuroCard ☐ American Express ☐ Discover

Card Number _____ Expiration Date_____

Cardholder Name _____ Signature _____

Organization _____ Telephone _____

Credit card orders may be faxed to (301) 634-7099 or emailed to staff@dues.faseb.org.

☐ Check or Money Order (US Currency Only - Drawn on US Bank)

Please send my subscription to:

Name_____ Organization_____

Address _____

City/State/ZIP-Postal Code _____

Telephone _____ Email _____

Mail to: *The FASEB Journal*, Dues & Subscriptions, Room L-2310, 9650 Rockville Pike, Bethesda, MD 20814-3998 USA

Call: 800-43-FASEB, Ext. 7029 (1-800-433-2732 x 7029 US only) or (301) 634-7029 **Fax:** (301) 634-7099

AUTHOR INSTRUCTIONS

Copyright Transfer and Publication Costs Approval Form

All authors are required to sign the following copyright transfer and cost agreement form prior to publication. **If you have not yet submitted this form to the editorial office, please fax it to 301-634-7809 as soon as possible.** Multiple forms may be submitted for the same article. Instructions for calculating publication charges are also attached for your convenience. Please read that sheet carefully. Do not fax your estimate sheet to the editorial office.

The FASEB Journal

The Journal of the Federation of American Societies for Experimental Biology

FASEB

Mandatory Copyright Transfer and Publication Costs Approval Form

Manuscript No.: _____

Title: _____

Author Names (Please Print All Names): _____

Signatures Below Certify Compliance With the Following Statements:

Copyright Transfer. In consideration of the acceptance of the above work for publication, I do herby assign and transfer to the Federation of American Societies for Experimental Biology (FASEB) all rights, titles, and interest in and to the copyright in *The FASEB Journal*. This includes preliminary display/posting of the abstract of the accepted article in electronic form before publication. The journal grants the author permission to provide a copy of the accepted manuscript to NIH upon acceptance for Journal publication, with public release in PubMed Central twelve months after final print publication by *The FASEB Journal*.

This form must be signed by all authors. If any changes in authorship (order, deletions, or additions) occur after the manuscript is submitted, agreement by all authors for such changes must be on file with FASEB. An author's name may only be removed at his/her own request and with written consent from all of the other authors, as well as final approval by the Editor-in-Chief. Material prepared by employees of the US Government in the course of their official duties cannot be copyrighted; work prepared by employees of the British or British Commonwealth government in the course of their official duties is subject to Crown Copyright and cannot be transferred to FASEB. Nevertheless, authors must sign the form to indicate acceptance of all terms other than copyright transfer.

○ Please check if this article was written as part of the official duties of an employee of the US government.
○ Please check if this article was written as part of the official duties of an employee of the British or British Commonwealth government.

Authorship Responsibilities. I attest that:

1. the manuscript is not currently under consideration, in press, or published elsewhere, and the research reported will not be submitted for publication elsewhere until a final decision has been made as to its acceptability by *The FASEB Journal* (posting of submitted material on a web site or by any other electronic means may be considered prior publication—note this in your cover letter);
2. the manuscript is truthful, original work without fabrication, fraud, or plagiarism;
3. I have made an important scientific contribution to the study and am thoroughly familiar with the primary data and;
4. I have read the complete manuscript and take responsibility for the content and completeness of the manuscript and understand that I share responsibility if the paper, or part of the paper, is found to be faulty or fraudulent.

Conflict of Interest Disclosure. All funding sources supporting the work and all institutional or corporate affiliations of mine are acknowledged. Except as disclosed on a separate attachment, I certify that I have no commercial associations (e.g., consultancies, stock ownership, equity interests, patent-licensing arrangements, etc.) that might pose a conflict of interest in connection with the submitted article, and that I accept full responsibility for the conduct of the trial, had full access to all the data, and controlled the decision to publish.

Author Fees. I agree to pay the following publication charges. Page charges are $80 per printed page for the first 8 pages; $160 per page for the 9th page and beyond. Color figures are $350 each. Articles containing eight or more figures and/or tables will be charged an additional $150 per figure and table. Supplemental files uploaded to the journal website are $100 for each file. All figures are in U.S. dollars.

Author Signatures. For more than 10 authors, use an extra sheet. Multiple forms are acceptable.

1. **Print Name:** _____ **Signature:** _____ **Date:** _____
2. **Print Name:** _____ **Signature:** _____ **Date:** _____
3. **Print Name:** _____ **Signature:** _____ **Date:** _____
4. **Print Name:** _____ **Signature:** _____ **Date:** _____
5. **Print Name:** _____ **Signature:** _____ **Date:** _____
6. **Print Name:** _____ **Signature:** _____ **Date:** _____
7. **Print Name:** _____ **Signature:** _____ **Date:** _____
8. **Print Name:** _____ **Signature:** _____ **Date:** _____
9. **Print Name:** _____ **Signature:** _____ **Date:** _____
10. **Print Name:** _____ **Signature:** _____ **Date:** _____

Signed forms should be faxed to 301-634-7809 or scanned and emailed to Mary Hayden at mhayden@faseb.org. E-mail questions to Mary Hayden at mhayden@faseb.org or call 301-634-7151.

AUTHOR INSTRUCTIONS

Calculating Publication Costs

The FASEB Journal now uses an online bill pay system for publication and reprint order fees. The corresponding author will receive a separate e-mail containing a link to a web page where charges can be paid by credit card. The e-mail link also will provide information about invoices, check payment, and wire transfers.

Publication charges are calculated based on the final version of the article and not this proof. Color figures have the word "COLOR" in the margins. Grayscale (black and white) figures have no tag. If you wish to change a color figure to grayscale, cross out the word "color" and write in "grayscale." Please note that figures are published the same way in the online and print versions of the journal. Authors may not publish figures in color online while publishing the same figures in grayscale in print or vice-versa. Authors wishing to reduce costs by combining supplemental files should contact Mary Hayden at mhayden@faseb.org.

For your convenience and records, the following table should help you estimate publication charges. Please account for any changes you have made to your proofs. **Please <u>do not</u> fax this sheet to the editorial office. Your charges will be calculated automatically based on the final article.**

	Quantity		Unit Price		Total
Per page cost, first 8 pages		×	$80 per page	=	
				+	
Per page cost, 9th page and beyond		×	$160 per page	=	
				+	
Color figures		×	$350 per figure	=	
				+	
Any combination of figures and/or tables over 7		×	$150 per figure or table	=	
				+	
Individual supplemental files		×	$100 per file	=	
			Total Publication Charges:		

This sheet is for estimation purposes only. Final costs are calculated using the final printed version of the article. All prices are in U.S. dollars. Open access fees are calculated separately. Reprints can be purchased when paying publication charges online.

AUTHOR INSTRUCTIONS

Page Proofs

Please review following article proof and fax corrections to: **1-717-738-9479.** Page proofs returned in any other way or faxed to any other number may lead to substantial publication delays. Please keep copies for your files.

Color figures have the word "COLOR" in the margins. Grayscale (black and white) figures have no tag. If you wish to change a color figure to grayscale, cross out the word "color" and write in "grayscale." (See below.) Publication charges will be calculated based on your changes to this proof. Please note that figures are published the same way in the online and print versions of the journal. Authors may not publish figures in color online while publishing the same figures in grayscale in print or vice-versa.

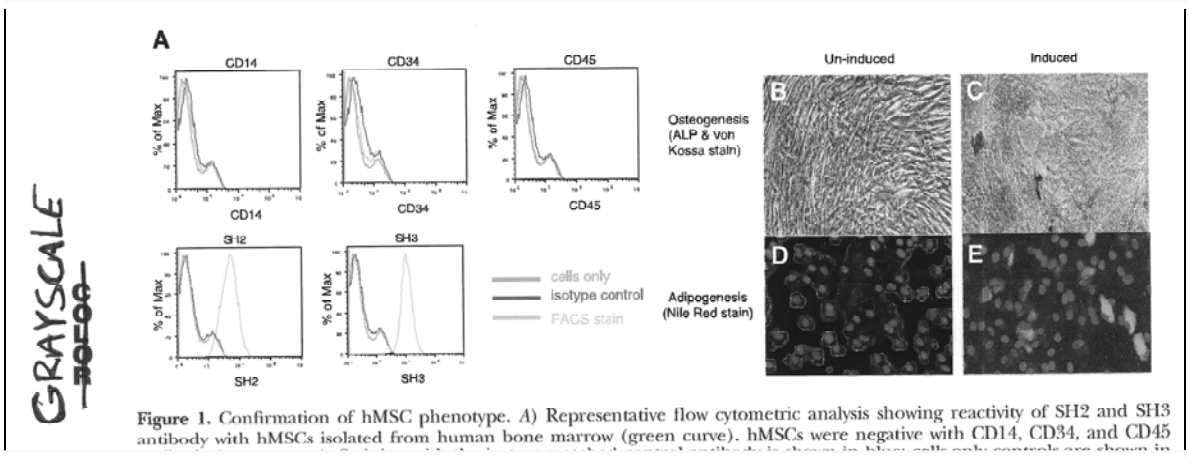

Figure 1. Confirmation of hMSC phenotype. *A*) Representative flow cytometric analysis showing reactivity of SH2 and SH3 antibody with hMSCs isolated from human bone marrow (green curve). hMSCs were negative with CD14, CD34, and CD45

NOTE: If you need to send new figure files to the editorial office, please draw an "X" through the figure and write "NEW FIGURE FILE REQUIRED" in the margin (see below). The editorial office will contact the corresponding author to obtain the necessary file(s).

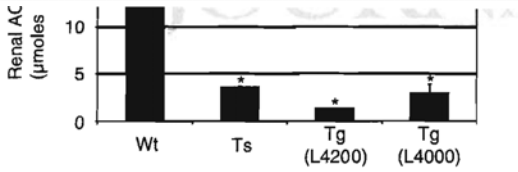

Figure 2. ACE activity assay. Age-matched, adult serum (*A*), lung extract (*B*), and kidney extract (*C*) were prepared from Wt and strain Ts, Tg (Line 4200) and Tg (Line 4000) mice as described in the Experimental Procedures. Lung or kidney protein extract (25 μg) or serum (1 μl) was assayed for ACE activity, measured as μmoles of His-Leu generated by cleavage of Ang I analog Hip-His-Leu in 1 h at 37°C. Each bar represents the average value from triplicate samples from five mice of the same genotype. Error bars indicate the 95% CI for each data sets. $*P \leq 0.001$ $**P \leq 0.0005$, $***P \leq 0.00005$ *vs.* Wt control strain mice.

sion in the Wt mouse. In contrast, as expected, transgenic sACE or gACE was not expressed in the proximal tubules (**Fig. 5**).

To correlate the level of ACE activity observed in the lung samples obtained from the Ts and Tg strain mice (Fig. 2) with the level of ACE produced in the vascular endothelial cells of these same strains, we repeated the

restored fertility (30). All of our other *Ace*−/− mice expressing sACE in sperm (Ps strain), or sACE in other somatic tissues (i.e., vasculature, kidneys or serum), remained sterile (29, 30). Similarly, male fertility was

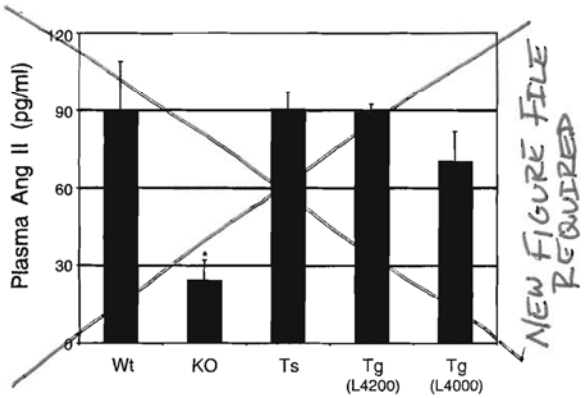

Figure 3. Plasma Ang II measurements. Plasma (1 ml) pooled from 4 adult mice of the same age, sex, and genotype was assayed for Ang II levels as described in Experimental Procedures. Each data point is the average of duplicate measure-

AUTHOR INSTRUCTIONS

Proofreader's Marks

Use a pen with black, blue, or red ink. Make two marks for every correction: one in text and one in the margin. A mark in text may be a caret (∧) or a line drawn through the character or word to be deleted. If there are several changes to be made in one line, arrange them in sequence left to right separated by a slash line. For the same correction repeated in one line, write the correction and a slash for each repetition (example: ∧, // to add two commas. For number corrections, slash through the wrong digits in the text, write the correct digits in the margin, and circle the correct number in the margin: 7880 52 (7520).

Mark	Meaning	Example	Result
‖	Align	‖← copyfitting	copyfitting
✓	Apostrophe	proofreaders marks	proofreader's marks
~~	Boldface	point	**point**
[/]	Brackets	letterspacing [/]	[letterspacing]
≡	Caps	caption	CAPTION
c/lc	Caps and lowercase	JUSTIFICATION c/lc	Justification
⊐⊏	Center	⊐column⊏	column
⬭	Change copy as indicated	eleven fonts use fig	11 fonts
⁀	Close up	head line	headline
:/	Colon	subhead :/	subhead:
⤴	Comma	indentation ,/	indentation,
℘	Delete	~~not~~ hardly	hardly
⁀	Delete and close up	kerning	kerning
em	Em dash	descender and	descender—and
!/	Exclamation point	ascender !/	ascender!
=/	Hyphen	demi bold	demi-bold
□	Indent	□character	character
∧	Insert	typeface library	typeface library
———	Italicize	leading	*leading*
/ lc	Lowercase	TYPOGRAPHY lc	typography
⊏	Move left	⊏composition	composition
⌐	Move right	text⌐	text
¶	New paragraph	display. Type	display. Type
(/)	Parentheses	roman (/)	(roman)
●	Period	backslant	backslant.
(?)	Query	itelic (? sp)	italic
?/	Question mark	boldface ?/	boldface?
“/”	Quotation marks	condensed	“condensed”
stet	Retain original	compressed stet	compressed
⊂	Run on	new faces ⊂are	new faces are
;/	Semicolon	expanded ;/	expanded;
≡ sc	Small caps	PUNCTUATION	PUNCTUATION
#	Space	linelength	line length
✓✓	Space evenly	in✓the✓news	in the news
⌒ tr	Transpose	runaround tr	runaround
⊗	Type is bad	visual ⊗	visual
⬭ wf	Wrong font	cursive wf	cursive

The FASEB Journal • Research Communication

Membrane structure and interactions of human catestatin by multidimensional solution and solid-state NMR spectroscopy

Masae Sugawara,*,[1] Jarbas M. Resende,*,†,[1] Cléria Mendonça Moraes,* Arnaud Marquette,* Jean-Francois Chich,‡,§ Marie-Hélène Metz-Boutigue,‡ and Burkhard Bechinger*,[2]

*Université de Strasbourg/Centre National de la Recherche Scientifique, UMR 7177, Institut de Chimie, Strasbourg, France; †Universidade Federal de Minas Gerais, Departamento de Química, Belo Horizonte, Brazil; ‡INSERM U575, Physiopathologie du Système Nerveux, Strasbourg, France; and §Institut National de la Recherche Agronomique, Virologie et Immunologie Moléculaires, Domaine de Vilvert, Jouy-en-Josas, France

AQ: 1

ABSTRACT **Catestatin is a natural peptide of higher organisms including humans, with a wide variety of biological functions involved in catecholamine inhibition, cardiovascular regulation, control of blood pressure, inflammation, and innate immunity. It is derived from the natural processing of chromogranin A, induced in the skin after injury, and produced by chromaffin cells and neutrophils. With neutrophils, the peptide enters the cell by crossing the plasma membrane where it interacts with internal targets to induce calcium influx. Therefore, we investigated the membrane interactions and structure of several catestatin-derived peptides. Whereas fluorescence dye release experiments are indicative of membrane permeabilization, multidimensional solution NMR and circular dichroism spectroscopies show that catestatin adopts α-helical conformations between Ser-6 and Tyr-12 in the presence of dodecylphosphocholine micelles. Furthermore, proton-decoupled ^{15}N solid-state NMR spectroscopy of sequences labeled with ^{15}N and reconstituted into oriented lipid bilayers indicates that this domain is aligned in a strongly tilted to inplanar alignment. Proton-decoupled ^{31}P NMR spectra of the same samples are indicative of conformational and/or orientational heterogeneity at the level of the lipid bilayer head groups due to the presence of catestatin. The sequence and 3-dimensional structure of catestatin exhibit homologies with Penetratin, which is suggestive that they both enter the cells by related mechanisms to target internal structures.—Sugawara, M., Resende, J. M., Moraes, C. M., Marquette, A., Chich, J.-F., Metz-Boutigue, M.-H., Bechinger, B. Membrane structure and interactions of human catestatin by multidimensional solution and solid-state NMR spectroscopy. *FASEB J.* 24, 000–000 (2010). www.fasebj.org**

Key Words: catestatin-derived peptides · cationic peptides · antimicrobial peptide · structure of membrane-associated peptide · oriented lipid bilayer · topology · angular restraints · membrane topology · cell-penetrating peptide

AQ: 2

Chromogranin a (CGA), the first member of the chromogranin/secretogranin family (1) is predominantly released with catecholamines by stimulated chromaffin cells from the adrenal medulla (2). CGA, a 48-kDa protein with several post-translational modifications (phosphorylation, *O*-glycosylation; refs. 3, 4), functions as a prohormone and generates several bioactive peptides (5). The *in vitro* as well as *in vivo* activities of the CGA-derived peptides (6) demonstrate their participation in homeostatic processes such as catecholamine release inhibition, calcium and glucose metabolisms, cardiovascular functions, inflammatory reactions (7, 8), pain relief, tissue repair, gastrointestinal motility, microglia, and activation and in the first line of defense against invading microorganisms by direct killing and activation of neutrophils (PMNs; ref. 9).

During the past decade, a range of antimicrobial peptides derived from the natural processing of chromogranins has been identified (10–13). These peptides result from the natural processing by intragranular enzymes such as prohormone convertases (PC1 and PC2), aminopeptidases, and carboxypeptidases; by kallikrein located at the outer membrane level (5); and by circulatory proteolytic enzymes such as plasmin and thrombin (14). Moreover, when PMNs accumulate at sites of inflammation and are stimulated by lipopolysaccharide or other microbial agents, these cells have emerged as a source of intact and processed forms of CGA (9, 10, 12).

Among these, bovine and human catestatin [$bCGA_{344–364}$ (bCAT) and $hCGA_{352–372}$ (hCAT)] are highly conserved during evolution (**Table 1**). Catestatins (CATs) are cationic peptides (hCAT, charge +4; bCAT, charge +5) initially characterized for their inhibitory effect on catecholamine release by chromaffin cells of the adrenal medulla (15, 16). These peptides display a noncom-

T1

[1] These authors contributed equally to this work.

[2] Correspondence: Bechinger, Faculté de chimie, Institut le Bel, 4, rue Blaise Pascal, 67070 Strasbourg, France. E-mail: bechinger@chimie.u-strasbg.fr

doi: 10.1096/fj.09-142554

TABLE 1. *Sequence alignment of CAT-derived peptides and Penetratin by using ClustalW*

Peptide	Sequence
Human (P10645)	352 SSMKLSFRARAYGFRGPGPQL 372
G364S	SSMKLSFRARAYSFRGPGPQL
P370L	SSMKLSFRARAYGFRGPGLQL
Macaque (Q4R4V1)	353 RSMKLSFRARAYGFRGPGPQL 373
Bovine (P05059)	344 RSMRLSFRARGYGFRGPGLQL 364
Bovine cateslytin	344 RSMRLSFRARGYGFR 358
Horse (Q9XS63)	343 RSMKLSFRARAYGFRGPGLQL 363
Pig (P04404)	343 RSMKLSFRAPAYGFRGPGLQL 363
Rat (P10354)	367 RSMKLSFRARAYGFRDPGPQL 387
Mouse (P26339)	364 RSMKLSFRTRAYGFRDPGPQL 384
ANTP (P02833)	339 RQIKIWFQNRRMKWKKENKTK 359
Drosophila	.::: *: * : :: .

Changes in human variants are underscored. Residue not included in the alignment is double underscored. Asterisk (*) indicates identical residues; period (.) and colon (:) indicate conservative changes.

petitive inhibition of the nicotinic acetylcholine receptor (15). When long ACh stimulation periods (30 s) are used during electrophysiological investigations, CAT inhibits ion translocation and it was proposed that this is due to interactions of the peptides at sites topographically distinct from ACh binding (17). Whereas a first site is located within the ion channel pore, a second one is located at the interface of the receptor within the membrane lipids (18, 19). Furthermore, in addition to the inhibition of catecholamine release, bCAT was found to act as a potent vasodilatator *in vivo* by stimulating the release of histamine (20). Such release of histamine was also demonstrated *in vitro* from mast cells, and the authors propose that CAT activates histamine release from mast cells by a mechanism analogous to the receptor-independent, peptidergic pathway proposed for mastoparan, as well as other cationic and amphipathic peptides (21). In addition, CAT was characterized as an endogenous antimicrobial peptide induced in skin after injury (22) and we have reported that bCAT and hCAT induce calcium entry in human neutrophils by calmodulin-regulated calcium-independent phospholipase A2 *via* store-operated channels (9). Furthermore, like other neuropeptides (beta-endorphin, met-enkephalin, substance P, somatostatin, vasoactive intestinal peptide, and neuropeptide Y), CAT mediates monocyte migration by a tyrosine kinase and a G-protein coupled receptor involving sphingosine-1-phosphate (23). The ensemble of these observations suggests the involvement of bCAT in innate immunity.

Genetic ablation of the CGA gene results in high blood pressure in mice, which can be rescued by either pretreatment with CAT or the introduction of the human CGA gene (24). Interestingly, 3 naturally occurring amino acid substitution variants within the CAT sequence were characterized (G364S, P370L, and R374Q) with allele frequencies of 4, 0.3, and 0.6%, respectively, the G364S variant causing profound changes in human autonomic activity and a possible decrease of risk to hypertension, especially in men. Recently, it was reported that cathepsin L, a proteolytic enzyme, colocalizes with chromogranin A in chromaffin vesicles to generate active peptides and that the processing of the CAT region was diminished by the 2 variants P370L and G364S (25).

The molecular mechanisms of the numerous biological activities of CAT indicate that, in addition to receptor-dependent mechanisms, this peptide is able to target various microorganisms such as bacteria, fungi, and parasites in the absence of a specific receptor (12) and also host cells such as neutrophils by a direct interaction with the plasma membranes. A prerequisite to understand the molecular interaction of natural hCAT and its variants (G364S and P370L) with various cellular membranes is the knowledge of the 3-dimensional structure and their interactions with phospholipids bilayers. Previous studies (26) have investigated the CAT 3-dimensional topology by homology modeling, suggesting that the peptide adopts a sheet-loop-sheet structure in aqueous environments. Furthermore, the structures in DMSO of hCAT and a cyclic engineered bCAT ($cbCGA_{350-362}$) were compared, indicating that the linear hCATpresents a coiled loop structure (PDB ID: 1LV4) and the $cbCGA_{350-362}$ adopts a twisted loop structure (PDB ID: 1N2Y; ref. 27).

To understand the possible molecular interactions of CAT with biological membranes, we decided to analyze the structure and topology of hCAT and its natural variants (G364S and P370L) in model membranes by circular dichroism (CD), as well as multidimensional solution- and solid-state NMR spectroscopies. The dodecylphosphocholine (DPC) micelles and phospholipid bilayers used in this study closely mimic the interfacial properties of biological membranes.

MATERIALS AND METHODS

Phospholipids were purchased from Avanti Polar Lipids (Birmingham, AL, USA). The CAT-derived peptides $bCGA_{344-364}$ RSMRLSFRARGYGFRGPGLQL, $hCGA_{352-372}$ SSMKLSFRARAYGFRGPGPQL, its human variants (G364S and P370L), and the scrambled peptide (SLPRRQLPSSAGMRGGKFAYF) were synthesized by automated solid-phase peptide synthesis using the Fmoc (9-fluorenylmethyloxycarbonyl) chemistry. At position 9 (underscored), the ^{15}N-labeled analog of alanine was incorporated. The synthetic peptides were purified using reversed phase high-performance liquid chromatography. The purity of the products was confirmed by sequencing and matrix-assisted laser desorption ionisation time of flight (MALDI-TOF) mass spectrometry.

Calcein release experiments

Large unilamellar vesicles (LUVs) loaded with calcein were prepared in the following manner: a lipid mixture of 1-palmitoyl-2-oleoyl-*sn*-glycero-3-phosphocholine/1-palmitoyl-2-oleoyl-*sn*-glycero-3-phosphoserine (POPC/POPS; 3:1) was dissolved in chloroform/methanol 1:1. The solution was dried and then hydrated in a 10 mM phosphate buffer (pH 5.5) complemented with 50 mM of calcein disodium salt (Fluka, Buchs, Switzerland) before undergoing several freeze-thaw cycles and then extrusion (21 times) through membranes with pores of 100 nm diameter (Avestin, Ottawa, ON, Canada). The dye outside the calcein-loaded vesicles was removed by gel filtration through a Sephadex G-50 column (2.5×3.5 cm; AQ: 3

Sigma, St. Louis, MO, USA) equilibrated with a 10 mM phosphate buffer (pH 5.5) and supplemented with 100 mM NaCl to compensate for the change in osmolarity induced by the presence of calcein and its sodium counter-ions. During gel filtration, the membranes were diluted by ~7-fold to a final lipid concentration of 3.5 mg/ml.

Calcein efflux measurements induced by peptides were performed on a Fluorolog 3–22 spectrometer (Horiba Jobin-Yvon, Longjumeau, France). In a typical experiment, LUV solution (6 μl) was added to 1.5 ml of 100 mM NaCl and 10 mM phosphate (pH 5.5) in a quartz cuvette and equilibrated for some minutes at room temperature inside the spectrometer. To start calcein release, an aliquot of peptide solution was added to the cuvette while the sample was excited at λ_{ex} = 480 nm, and the intensity of fluorescence (I) was recorded at λ_{em}= 515 nm for 10 min. A limited bandwidth (λ<1.2 nm) was used for both excitation and emission. The percentage of calcein released from the vesicles ($I_{\%}$) was calculated according to the formula $I_{\%} = 100 \cdot (I - I_0)/(I_{max} - I_0)$, where I_0 represents the intensity of fluorescence before adding the peptide to the solution and I_{max} is the maximum intensity observed after fully disrupting the vesicles with 10 μl of 10% Triton X-100.

CD spectroscopy

To record CD spectra, the peptides were dissolved at 0.25 mg/ml in 10 mM phosphate buffer (pH 5.5). For detergent-containing samples, the appropriate volume of an 800 mM DPC stock solution was added to obtain the final DPC concentration of 10, 100, 200, or 400 mM, respectively. The CD spectra were recorded on a Jasco J 810 spectrometer (Jasco, Inc., Easton, MD, USA) at 298 K. The path length of the sample cell quartz cuvette was 1 mm (Hellma, Müllheim, Germany), and 8 acquisitions were accumulated for each spectrum. The step resolution was 1 nm at a scanning speed of 200 nm/s with 1 s response time.

After subtraction of the buffer/detergent control, the CD spectral intensities in the range 190–250 nm were converted to mean residue ellipticity. The secondary structure elements were estimated using the DICHROPROT software package (28) implemented on a personal computer.

Mutidimensional solution NMR spectroscopy

For solution NMR spectroscopy, 2.9 mg of the lyophilized powder of G364S was dissolved in MilliQ water at a final concentration of 2 mM in 400 mM DPC-d_{38} (Cambridge Isotope Laboratory, Andover, MA, USA), 0.01% NaN_3 (w/v), 5% D_2O (v/v), and 10 mM phosphate buffer (pH 5.5). One- and 2-dimensional NMR experiments were performed at 298 K on a DRX500 spectrometer (Bruker Biospin; Bruker, Karlsruhe, Germany) equipped for pulsed field gradient spectroscopy. For ^{1}H assignments, 2-dimensional homonuclear total correlation spectroscopy (TOCSY), nuclear Overhauser enhancement spectroscopy (NOESY), and double-quantum filtered correlation spectroscopy (DQF-COSY) spectra were recorded (see ref. 29 for references). The TOCSY experiments were performed with a mixing time of 60 ms using the decoupling in the presence of scalar interactions (DIPSI)-2 sequence and phase sensitive echo-antiecho gradient selection. The mixing times of the NOESY experiments were 100 and 200 ms. NOESY and DQF-COSY spectra were recorded by using the States-time-proportional phase incrementation (TPPI) phase-sensitive method. The water signal was suppressed by using the WATERGATE sequence in combination with presaturation during the relaxation delay for all recorded spectra. For these experiments, 8–24 transients for 512 t_1 increments with 2048 (TOCSY and NOESY) or 4096 (DQF-COSY) complex data points were collected. The spectral width was set to 4310 Hz for DQF-COSY and DIPSI and 5000 Hz for NOESY spectra in both dimensions, and the relaxation delay between successive transients was 2 s. All solution NMR spectra were processed with NMRPIPE (30). Since the peptide G364S was selectively labeled with ^{15}N, each NMR spectrum was recorded twice, once with and once without ^{15}N decoupling during acquisition.

NOE data analysis and structure calculations

The NMR spectra were analyzed using NMRVIEW 5.0.3 (31). NOE intensities obtained at 200 ms mixing time were converted into semiquantitative distance restrains using the calibration previously reported by Hyberts *et al.* (32). The upper limits of the distances restrains thus obtained were 2.8, 3.4, and 5.0 Å (strong, medium, and weak NOE, respectively). Structure calculations were performed using the Xplor-NIH 2.14.0 software (33). Starting with an extended conformation, 100 structures were generated using a simulated annealing protocol. This was followed by 15000 steps of simulated annealing at 1000 K and a subsequent decrease in temperature in 14000 steps in the first slow-cool annealing stage. The display, analysis, and manipulation of the 3-dimensional structures were performed with the program MOLMOL (34). The atomic coordinates of the most stable structures have been deposited in the Biological Magnetic Resonance Data Bank (BMRB; accession no. 20080; http://www.bmrb.wisc.edu). AQ: 4

Solid-state NMR measurements

Oriented membrane samples were prepared as described previously (29). In short, the peptide and the lipids were codissolved, and the mixtures were applied onto 30 ultrathin coverglasses (9×22 mm; Paul Marienfeld GmbH & Co., KG, Lauda-Königshofen, Germany) that were first dried in air and thereafter in high vacuum overnight. After the samples had been equilibrated at 93% relative humidity, the glass plates were stacked on top of each other. The stacks were stabilized and sealed with Teflon tape and plastic wrappings.

Proton-decoupled ^{15}N solid-state NMR spectra were acquired on a Bruker AMX400 wide-bore NMR spectrometer using a commercial double-resonance solid-state NMR probe modified with flattened coils (35) of inner dimensions 15 × 9 × 4 mm^3. Measurements were carried out at sample orientations with the glass plate normal parallel or to the magnetic field direction. A cross-polarization sequence with an adiabatic shape for the ^{15}N irradiation was applied with the following typical acquisition parameters: 90° pulse width of 8 μs, spin lock time of 700 μs, recycle delay of 3 s, 512 data points, 33,000 acquisitions, and spectral width of 33 kHz (36). NH_4Cl was used as an external reference (41.5 ppm). Before Fourier transformation, an exponential apodization function corresponding to a line broadening of 300 Hz was applied.

Proton-decoupled ^{31}P solid-state NMR spectra of the oriented phospholipid samples were recorded at 162.0 MHz on a Bruker AMX400 wide-bore NMR spectrometer using a commercial double-resonance solid-state NMR static probe. A Hahn echo pulse sequence was used for spectral acquisitions (37). The following spectral parameters were used: spectral width of 75 kHz, acquisition time of 13.6 ms, 2048 time domain data points, 90° pulse width of 2.5 μs, echo delay of 40 μs, recycle delay of 5 s, and 128 scans. H_3PO_4 at 85% was used as external reference (0.0 ppm). Before Fourier transformation, an exponential apodization function corresponding to a line broadening of 100 Hz was applied.

RESULTS

In a first step, the membrane interactions and permeabilizing activities of bCAT (18 μM) and hCAT (20 μM), including the wild-type peptide and the 2 mutants (18 μM G364S and 16 μM P370L), were tested (**Fig. 1**). When these peptides were added to calcein-loaded POPC/POPS 3:1 vesicles, the dye was released within minutes and diluted in the environment concomitant with an increase in fluorescence intensity. In contrast, the fluorescence signal remained constant when the scrambled peptide sequence was added to lipid membranes (data not shown). It is also apparent that the effect is more pronounced for the 2 mutants of hCAT when compared with the wild-type peptide, suggesting a crucial role of S364 and L370, as well as for bCAT which is different at position R344 (Table 1).

In a next step, CD measurements of hCAT and its derived peptides were performed in the presence of detergents. CD spectroscopy provides global information on the content of α-helical, β-sheet, and random coil structures and is therefore well suited to screen the chemical environments that promote the formation of secondary structures and that are best suited for an NMR spectroscopic analysis. Whereas in the absence of membranes the 4 peptides show only weak dichroic signals in the range 190–250 nm (**Fig. 2**), negative intensities at 209 and 222 nm indicate the formation of some helical structure in the presence of detergent micelles (Fig. 2). The α-helix content increases when ≥50 mM of the zwitterionic detergent DPC is added. At this detergent concentration, the maximum helix content of hCAT, bCAT, and G364S is ~20 ± 5%, whereas the P370L mutant seems to attain somewhat larger values.

The structural transition between the random coil conformation of the peptide free in solution and the α-helical structure when associated with membranes allows one to estimate the membrane partitioning

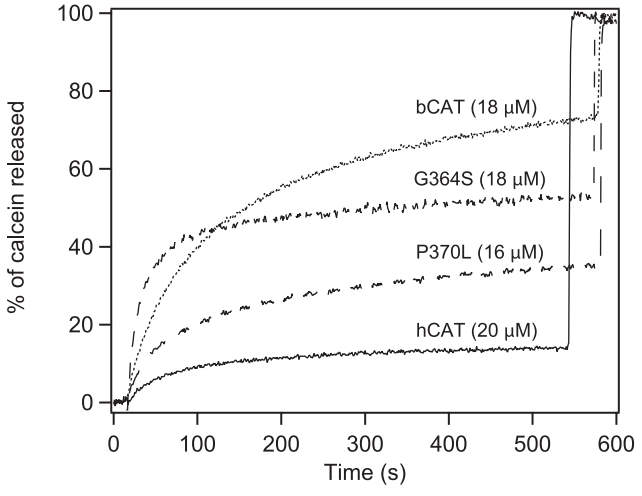

Figure 1. Calcein release from anionic vesicles (POPC/POPS=3/1) induced by human CAT, by its 2 variants P370L and G364S, and by bCAT. Measurements were made in a 100 mM NaCl, 10 mM phosphate buffer (pH 5.5), and lipid concentration corresponds to 25 μM.

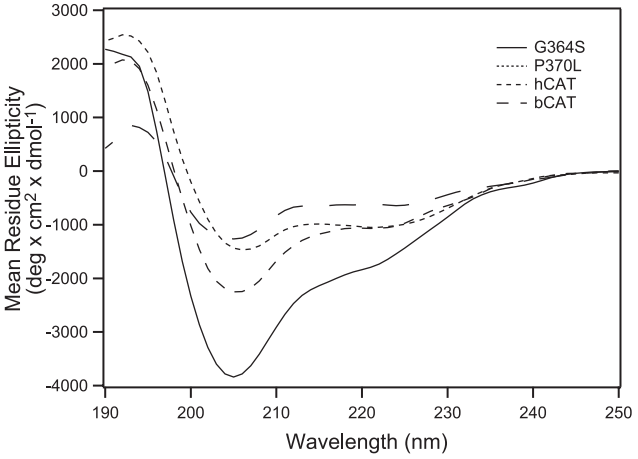

Figure 2. CD spectra of CATs in the presence of 100 mM DPC (10 mM phosphate buffer, pH 5.5).

constant K_p according to $K_p = P_b/P_f \cdot L$, where P_f, P_b, and L are the concentrations of free peptide, bound peptide, and lipid (or detergent), respectively. With a transition midpoint ($P_b=P_f$) <50 mM DPC, K_p is >20 M^{-1}. Furthermore, when peptides were added to vesicles containing PG and/or sterols and the resulting complexes were precipitated by centrifugation, the partitioning of peptide between the pellet and the supernatant was indicative of $K_p \leq 3500\ M^{-1}$ (data not shown). These values suggest that only a small fraction of peptides associates with zwitterionic lipid bilayers, which is in agreement with channel measurements, but that the P_b/P_f ratio is increased when high lipid/detergent concentrations, such as in the NMR structural studies (see below), or negatively charged membranes are used (Fig. 1). In the latter case, the concentration of cationic peptides close to the membrane is increased due to electrostatic attraction and increases of the apparent partitioning constant of up to 2–3 orders of magnitude have been observed for cationic sequences (38). By taking such effects into account the ratio of membrane peptide-to-lipid ratio was estimated to be ≤1:100 in case of POPC/POPS membranes used in the calcein release experiments (Fig. 1).

The CD spectroscopic investigations of the peptides indicate that relatively high concentrations of detergent are needed for the full association of the peptide with zwitterionic membranes. Because the G364S variant causes profound changes in human autonomic activity, reduces the risk of developing hypertension, represents the major variant with a frequency of 3–4%, and occurs at a highly conserved site among mammalian CAT sequences (Table 1) and has the highest propensity to adopt secondary structures (Fig. 2), we decided to analyze in detail the membrane-associated conformation and topology of this variant.

As a consequence, the peptide G364S was further investigated by multidimensional ^{1}H solution NMR spectroscopy at a peptide/detergent ratio of 1:200 in the presence of 400 mM DPC, *i.e.*, a detergent concentration where all 4 peptides exhibit stable secondary structures (Fig. 2). This technique allows for the detailed structural investigation of peptides and proteins

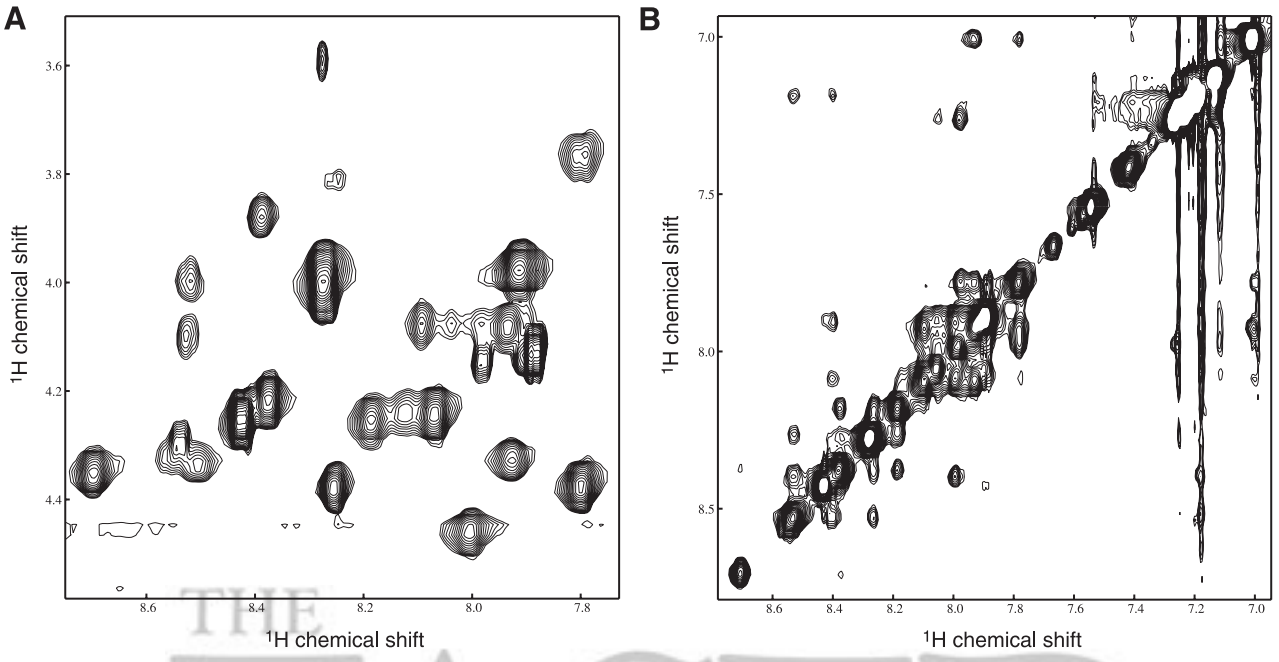

Figure 3. Fingerprint region (HN-Hα correlations) of TOCSY spectrum (*A*) and amide proton cross-peak region of NOESY spectrum (*B*) of G364S in 400 mM DPC micelles (10 mM phosphate buffer, pH 5.5, at 298 K).

in aqueous and micellar environments. Selected spectral regions of TOCSY and NOESY spectra are shown in **Fig. 3**, and the resulting ^{1}H-^{1}H correlations were used for the assignment of all signal intensities. The uniform spectral properties and the number of spin systems corresponding to the number of amino acid residues indicate a homogenous structure at the NMR time scale at the conditions used for this experiment (Fig. 3).

In the presence of DPC micelles, interresidue HN-HN NOEs are observed throughout the sequence (**Fig. 4**), indicating close distances between the amide protons (≤5 Å). Furthermore, several medium range NOEs are indicative for an α-helical structure encompassing residues 6 to 12 (corresponding to residues S357 to Y363 of hCAT). When the NOE information was used in simulated annealing and distance geometry calculations, a family of structures with α-helical conformations in the central region of the peptide wass obtained (**Fig. 5**). The root mean square deviation values calculated with MOLMOL (34) of the helical segment are 0.28 for the backbone atoms and 0.86 for backbone and heavy atoms.

Whereas 2-dimensional solution NMR spectroscopy of G364S associated with DPC micelles provides a good indication of the conformational details of this peptide in membrane interfaces, the interactions of CATs with bilayers and their membrane topology were further investigated using solid-state NMR spectroscopy. This technique has the proven potential for the structural analysis of polypeptides associated with phospholipid bilayers (39–42) as well as the study of their membrane interactions in a lipid-dependent manner (43–48). Notably, the solid-state NMR method is unique in that it is capable of obtaining details on the polypeptide alignment relative to the membrane at near physiological conditions (49, 50). This approach consists in preparing peptides that have been labeled with ^{15}N at one or several amide positions and reconstituted into oriented membranes (42). Therefore, to analyze the membrane topology of hCAT, G364S, and P370L, the alanine-9 positions (corresponding to A360) were labeled with ^{15}N, *i.e.*, well within the helical region when the G364S peptide is associated with DPC micelles (Figs. 4 and 5), and the peptides were reconstituted into oriented phospholipids bilayers at peptide-to-lipid ratios of 1:100. The ^{15}N chemical shift measured from such samples provides a direct and convenient measure of the approximate tilt angle of the ^{15}N-H vector and thereby also of α-helical domains relative to the membrane normal (51). Whereas chemical shift values in

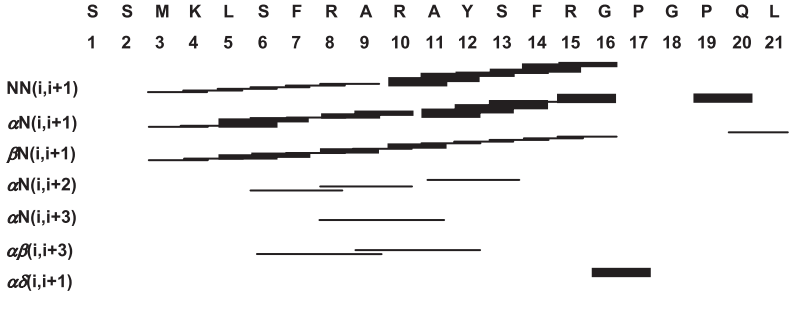

Figure 4. Graphical representation of the NOE cross peaks of G364S in 400 mM DPC micelles (10 mM phosphate buffer, pH 5.5, at 298 K).

COLOR

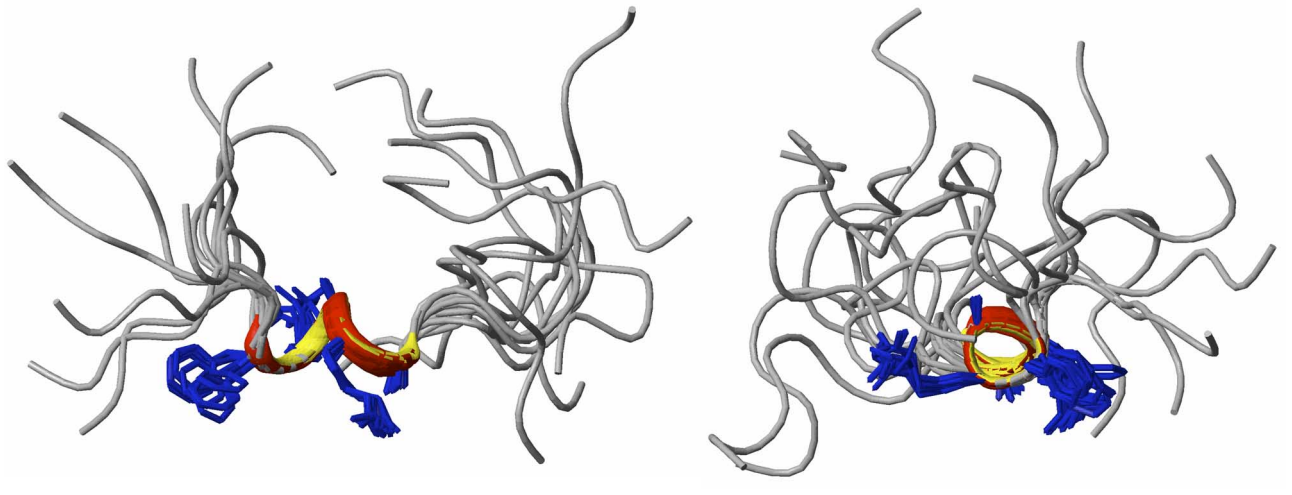

Figure 5. Top panel: backbone alignment of the global fold of the 10 lowest energy structures of G364S in the presence of 400 mM DPC (10 mM phosphate buffer, pH 5.5, at 298 K). Bottom panel: side-chain residues of the helical segment (aa 7–11) are shown in blue. NMR structures are oriented to show the N terminus facing to the left (left panel) and to the front (right panel).

the 200-ppm range are indicative of transmembrane topologies, resonances <100 ppm correlate with alignments parallel to the membrane surface (51). The ^{15}N solid-state NMR spectra of all 3 hCAT peptides show ^{15}N chemical shift intensities in the 125-ppm region, a value indicative of a strongly tilted helix relative to the membrane normal or a site that shows high flexibility, including conformational exchange or fast reorientation of the whole molecule (**Fig. 6*B*, *C***). In addition, the signal intensity of the G364S mutant extends well into the region <100 ppm (maximum at 93 ppm). Such chemical shift values are indicative of a predominant alignment of the ^{15}N-H vector close to parallel to the membrane surface (Fig. 6*A*). Therefore, the ^{15}N spectra of the G364S peptide are indicative of topological/conformational exchange.

F6

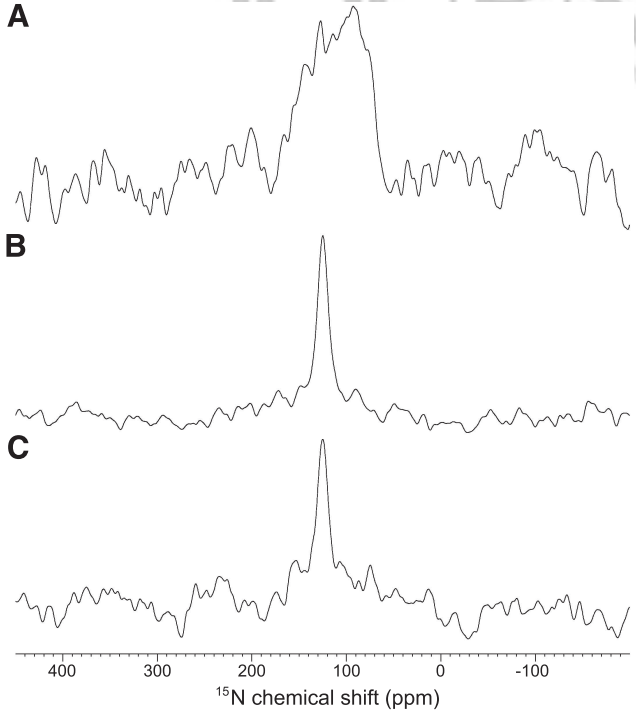

Figure 6. Proton-decoupled ^{15}N solid-state NMR spectra of G364S (*A*), P370L (*B*), and wild-type (*C*) reconstituted into oriented POPC bilayers at ambient temperatures. *A, B*) Peptide-to-lipid ratios are 1:100; ~60,000 scans. *C*) Peptide-to-lipid ratio is 1:68; 30,000 acquisitions were recorded.

The ^{31}P solid-state NMR spectrum of the same samples shows a predominant signal at 30 ppm with considerable signal intensities ranging to −15 ppm, *i.e.*, within a chemical shift distribution typical for liquid crystalline phosphatidylcholine bilayers (**Fig. 7**). Similar to the ^{15}N solid-state NMR approach mentioned above (Fig. 6), the ^{31}P chemical shift of the phospholipids depends on the alignment of the lipid molecules relative to the magnetic field direction of the spectrometer, and therefore the spectra shown in Fig. 7 allow one to evaluate the orientational and/or conformational order at the level of the phospholipid head groups (42). The line shape indicates that although the fluid disordered phase lipids are predominantly oriented with their long axes parallel to the magnetic field direction/glass plate normal, the peptides cause considerable structural/topological heterogeneity at the level of the phospholipid head groups.

F7

DISCUSSION

The mammalian peptide CAT is of considerable interest as a neuropeptide with an important role in the control of blood pressure, direct cardiovascular actions (52), and innate immunity (12, 22). Widespread antibacterial and antifungal properties have also been characterized for cateslytin (bCGA$_{344-358}$), a shorter homologue of human CAT (Table 1) encompassing the active domain of bCAT (12), and recent biophysical experiments indicate that it strongly interacts with membranes, where it causes pore formation (48, 53). Whereas the biological activities of the CAT peptides have been well characterized, little is known about their

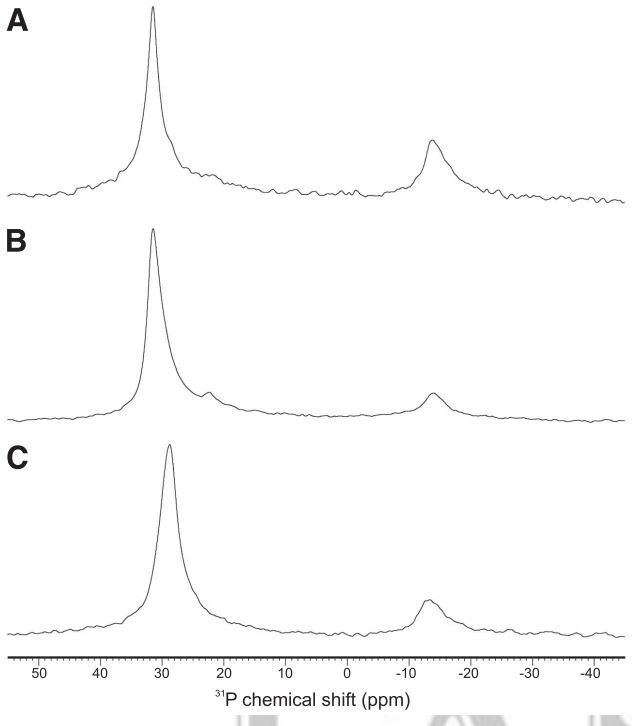

Figure 7. Proton-decoupled ^{31}P solid-state NMR spectra of oriented POPC membranes encompassing G364S (*A*), P370L (*B*), and the wild-type sequence hCAT (*C*) reconstituted at peptide-to-lipid ratios of 1:100. Temperature was 298 K. For comparison, close to perfect alignment of the phospholipid head groups is observed in the presence of more hydrophobic peptide sequences, as evident in the ^{31}P NMR spectra shown in Fig. 3 in Salnikov *et al.* (82).

peptide-membrane interactions and how they enter the cell interior.

When the amino acid composition of CAT (SSMKLS FRARAYGFRGPGPQL) is analyzed its membrane interaction is not obvious, *e.g.*, by the presence of an extended hydrophobic region or by an amphipatic structure. However sequence alignment of hCAT with Penetratin, an R-rich cell-penetrating peptide (CPP), indicates ≥60% homology, in particular when the N-terminal part is considered (Table 1), suggesting that CAT penetrates into cells by using a similar mechanism (9). Furthermore, it has recently been pointed out that cationic antimicrobial peptides and CPPs form a continuous spectrum of activities (54). This analysis suggests that CAT is related to other antimicrobial peptides that also exhibit CPP characteristics (55–58).

Additional parallels with some CPPs were revealed when we investigated the structure of CAT-derived peptides as well as their topology in membrane environments by CD, multidimensional solution, and solid-state NMR spectroscopies. The CD and NMR data indicate that CAT is largely unstructured in aqueous solution but forms a short helical conformation in the presence of high concentrations of DPC. The helix extends from residues 7 to 11, with additional medium-range contacts involving S6 and Y12 (corresponding to residues 357–363 of hCGA). The short helix observed in multidimensional NMR spectroscopy thus agrees well with the CD spectroscopy analysis, where a helix content of ~18% was measured. Although the variants investigated here exhibit some differences in their propensity to form helical structures, they all reach related degrees of helicity at high detergent concentrations (Fig. 2). The data thereby agree with previously published work on bovine cateslytin (CGA344-358), which predominantly adopts random coil conformations in aqueous solutions. However, the helix-forming propensity of the latter is less pronounced (59). The reasons for this are probably the differences in sequence (Table 1) and the cleavage of the peptide at R15, *i.e.*, not even a full turn away from the helical domain (S6 to Y12). Furthermore, it is noteworthy that the nicotinic cholinergic antagonist activity of bovine CGA is associated with residues 344–358 (27), thereby encompassing the region homologous to the one found helical in this work on the human sequence (Figs. 4 and 5 and Table 1).

Short helical structures flanked by predominantly random coil conformations have also been observed in the presence of SDS micelles for other R-rich sequences, such as penetratin (PAntp) (60), which is oriented parallel to the micellar surface (61). In addition, this peptide exhibits β structures at high peptide-to-lipid ratios or in the presence of acidic phospholipids (62). In a related manner, bovine cateslytin adopts β-sheet conformations when in contact with negatively charged interfaces (48, 53). In this context, the peptide has been shown to cause the separation of rigid and fluid membrane domains, and the resulting phase boundaries have been suggested to facilitate membrane crossing (47, 48). The CPPs dynorphin A and B have also been shown to interact with membranes; the N terminus of the former exhibits a tendency to adopt helical conformations (encompassing ~5 residues), which insert into the hydrophobic part of the membrane at an angle of 21° (62, 63).

In contrast, a number of other CCPs have been shown to form amphipathic helices, including calcitonin-derived peptides (63), transportan (64), or Pep-1, a lysine-rich sequence (65), and thereby resemble the membrane-associated structure of linear cationic antimicrobial peptides (50, 66–68). Overall, it seems that a particular structure or distribution of the positive charges is not a prerequisite for cell-penetrating activities (69, 70).

The ^{31}P and ^{15}N solid-state NMR data shown in Figs. 6 and 7 indicate that the region encompassing the short helix in the solution NMR structure interacts with phospholipid membranes and causes considerable disordering at the level of the phospholipid head groups. In the case of P370L and the wild-type sequence, the ^{15}N chemical shift is indicative of a tilted alignment relative to the membrane surface or close-to-isotropic mobility of position A360, but orientational or/and conformational heterogeneity is observed for G364S, with added signal intensities that agree with helical domains oriented approximately parallel to the membrane surface (51). In contrast, cationic amphipathic antimicrobial peptides have been found to be oriented parallel to the membrane surface in a stable fashion (a recent example is presented in ref. 29). Despite the structural differences, both cationic antimicrobial pep-

tides (49, 50, 71, 72) and several CPPs were found to induce membrane curvature strain (69, 73, 74). The topological and/or conformational heterogeneity at the level of the phopspholipid head groups, as evidenced by the ^{31}P NMR spectra shown in Fig. 6, probably reflects a similar activity also for the CAT-derived peptides investigated here. Simulations indicate that spectral line shapes similar to those shown in Fig. 6 arise from torroidal pore geometries (75), just to mention one possibility. As peptides at tilted angles intermediate to transmembrane and in plane have been suggested to have the highest effect on bilayer packing (76), one might speculate that the strongly tilted arrangement compensates for the shortness of the helical region of CAT-derived peptides.

Two of the five residues of the helical region of CAT are arginine, an amino acid that has been proposed to form hydrogen bonding interactions with phospholipids, thereby providing a hint on how this charged residue can pass across and help other sequences to transfer through the hydrophobic membrane barrier. Indeed the translocation properties of Arg containing CPPs have been shown to be directly associated with the presence of this amino acid (77). Furthermore, bidendate hydrogen bonding between the guadinium groups of protegrin, an R-rich antimicrobial peptide, and the phosphate groups of the bilayer has been demonstrated to be crucial for insertion and pore formation within bacterial membranes (78). The high density of arginines has been suggested to also form the basis for membrane interactions of other CPPs, such as R_n and Tat (54, 70).

Notably, the increase in membrane permeability for calcein is modest and occurs only at relatively high peptide concentrations (Fig. 1). Furthermore, when the 4 peptides of this study are compared with each other, the membrane permeability increases (bCAT≥G364S>P370L>hCAT; Fig. 1) do not directly correlate with the helix-forming propensity in the presence of DPC (Fig. 2). Indeed, modeling and molecular dynamics simulations indicate that membrane permeability increases do not necessarily involve a well-defined secondary structure nor the arrangement of the molecules in defined supramolecular aggregates (53, 79). However, it should be noted that pore formation and cell-penetrating activities probably require different conformational features, although both types of activities may very well be associated with a given peptide sequence (54). The ensemble of data therefore suggests that the peptides are capable of crossing the membrane without killing the target cells and that this activity requires different structural features. In this context, the variability in the peptide structure (Fig. 2) and topology (Fig. 6*A*) as well as its high degree of flexibility (Fig. 5) may be prerequisites to develop such a dual functionality. Once CATs reach the cell interior they interact with calmodulin (9), and they may well target other internal structures and molecules in order to develop antimicrobial activities, as has been observed with other antimicrobial peptides (80, 81), to stimulate immune cells, and to carry bioactive cargos inside cells. Fj

The authors thank Jesus Raya and Roland Graff for help with the solid-state and solution NMR spectrometers and Bernard Guérold (INSERM U575) for the peptide syntheses. This study was funded by INSERM, Institut National de la Recherche Agronomique (INRA), the University of Strasbourg, and the Centre National de la Recherche Scientifique (CNRS). Furthermore, the CNRS, CAPES, and CNPq are acknowledged for postdoctoral fellowships to M.S., C.M.M, and J.M.R., respectively. We thank Vaincre la Mucoviscidose (TG0602), the RMN Grand-Est Network of the Ministry of Recherche, and the European Commission under the 6th Framework Programme (Biocontrol, MCRTN-33439) for supporting the projects. We also thank the Brazilian-French program CAPES-COFECUB/EGIDE (487/05), which permitted several exchange visits to promote this work. The Institute for Supramolecular Chemistry of the University of Strasbourg (ISIS) is acknowledged for hosting the Bechinger Laboratory. AQ: 5

REFERENCES

1. Banks, P., and Helle, K. (1965) The release of protein from the stimulated adrenal medulla. *Biochem. J.* **97,** 40C–41C
2. Simon, J. P., and Aunis, D. (1989) Biochemistry of the chromogranin A protein family. *Biochem. J.* **262,** 1–13
3. Strub, J. M., Sorokine, O., Van, D. A., Aunis, D., and Metz-Boutigue, M. H. (1997) Phosphorylation and O-glycosylation sites of bovine chromogranin A from adrenal medullary chromaffin granules and their relationship with biological activities. *J. Biol. Chem.* **272,** 11928–11936
4. Gadroy, P., Stridsberg, M., Capon, C., Michalski, J. C., Strub, J. M., Van, D. A., Aunis, D., and Metz-Boutigue, M. H. (1998) Phosphorylation and O-glycosylation sites of human chromogranin A (CGA79-439) from urine of patients with carcinoid tumors. *J. Biol. Chem.* **273,** 34087–34097
5. Metz-Boutigue, M. H., Garcia-Sablone, P., Hogue-Angeletti, R., Aunis, D. (1993) Intracellular and extracellular processing of chromogranin A. Determination of cleavage sites. *Eur. J. Biochem.* **217,** 247–257
6. Helle, K. B., Corti, A., Metz-Boutigue, M. H., and Tota, B. (2007) The endocrine role for chromogranin A: a prohormone for peptides with regulatory properties. *Cell. Mol. Life Sci.* **64,** 2863–2886
7. Ferrero, E., Scabini, S., Magni, E., Foglieni, C., Belloni, D., Colombo, B., Curnis, F., Villa, A., Ferrero, M. E., and Corti, A. (2004) Chromogranin A protects vessels against tumor necrosis factor alpha-induced vascular leakage. *FASEB J.* **18,** 554–556
8. Blois, A., Srebro, B., Mandala, M., Corti, A., Helle, K. B., and Serck-Hanssen, G. (2006) The chromogranin A peptide vasostatin-I inhibits gap formation and signal transduction mediated by inflammatory agents in cultured bovine pulmonary and coronary arterial endothelial cells. *Regul. Pept.* **135,** 78–84
9. Zhang, D., Shooshtarizadeh, P., Laventie, B. J., Colin, D. A., Chich, J. F., Vidic, J., de, B. J., Chasserot-Golaz, S., Delalande, F., Van, D. A., Schneider, F., Helle, K., Aunis, D., Prevost, G., and Metz-Boutigue, M. H. (2009) Two chromogranin a-derived peptides induce calcium entry in human neutrophils by calmodulin-regulated calcium independent phospholipase A2. *PLoS ONE* **4,** e4501
10. Lugardon, K., Raffner, R., Goumon, Y., Corti, A., Delmas, A., Bulet, P., Aunis, D., and Metz-Boutigue, M. H. (2000) Antibacterial and antifungal activities of vasostatin-1, the N-terminal fragment of chromogranin A. *J. Biol. Chem.* **275,** 10745–10753
11. Lugardon, K., Chasserot-Golaz, S., Kieffer, A. E., Maget-Dana, R., Nullans, G., Kieffer, B., Aunis, D., Metz-Boutigue, M. H. (2001) Structural and biological characterization of chromofungin, the antifungal chromogranin A-(47–66)-derived peptide. *J. Biol. Chem.* **276,** 35875–35882
12. Briolat, J., Wu, S. D., Mahata, S. K., Gonthier, B., Bagnard, D., Chasserot-Golaz, S., Helle, K. B., Aunis, D., and Metz-Boutigue, M. H. (2005) New antimicrobial activity for the catecholamine release-inhibitory peptide from chromogranin A. *Cell. Mol. Life Sci.* **62,** 377–385
13. Strub, J. M., Garcia-Sablone, P., Lonning, K., Taupenot, L., Hubert, P., Van, D. A., Aunis, D., and Metz-Boutigue, M. H. (1995) Processing of chromogranin B in bovine adrenal medulla. Identification of secretolytin, the endogenous C-terminal

fragment of residues 614–626 with antibacterial activity. *Eur. J. Biochem.* **229,** 356–368
14. Biswas, N., Vaingankar, S. M., Mahata, M., Das, M., Gayen, J. R., Taupenot, L., Torpey, J. W., O'Connor, D. T., and Mahata, S. K. (2008) Proteolytic cleavage of human chromogranin a containing naturally occurring catestatin variants: differential processing at catestatin region by plasmin. *Endocrinology* **149,** 749–757
15. Mahata, S. K., O'Connor, D. T., Mahata, M., Yoo, S. H., Taupenot, L., Wu, H., Gill, B. M., and Parmer, R. J. (1997) Novel autocrine feedback control of catecholamine release. A discrete chromogranin a fragment is a noncompetitive nicotinic cholinergic antagonist. *J. Clin. Invest.* **100,** 1623–1633
16. Lee, J. C., Taylor, C. V., Gaucher, S. P., Toneff, T., Taupenot, L., Yasothornsrikul, S., Mahata, S. K., Sei, C., Parmer, R. J., Neveu, J. M., Lane, W. S., Gibson, B. W., O'Connor, D. T., and Hook, V. Y. (2003) Primary sequence characterization of catestatin intermediates and peptides defines proteolytic cleavage sites utilized for converting chromogranin a into active catestatin secreted from neuroendocrine chromaffin cells. *Biochemistry* **42,** 6938–6946
17. Herrero, C. J., Ales, E., Pintado, A. J., Lopez, M. G., Garcia-Palomero, E., Mahata, S. K., O'Connor, D. T., Garcia, A. G., and Montiel, C. (2002) Modulatory mechanism of the endogenous peptide catestatin on neuronal nicotinic acetylcholine receptors and exocytosis. *J. Neurosci.* **22,** 377–388
18. Lena, C., and Changeux, J. P. (1993) Allosteric modulations of the nicotinic acetylcholine receptor. *Trends Neurosci.* **16,** 181–186
19. Galzi, J. L., Changeux, J. P. (1995) Neuronal nicotinic receptors: molecular organization and regulations. *Neuropharmacology* **34,** 563–582
20. Kennedy, B. P., Mahata, S. K., O'Connor, D. T., and Ziegler, M. G. (1998) Mechanism of cardiovascular actions of the chromogranin A fragment catestatin in vivo. *Peptides* **19,** 1241–1248
21. Kruger, P. G., Mahata, S. K., Helle, K. B. (2003) Catestatin (CgA344–364) stimulates rat mast cell release of hi and stamine in a manner comparable to mastoparan and other cationic charged neuropeptides. *Regul. Pept.* **114,** 29–35
22. Radek, K. A., Lopez-Garcia, B., Hupe, M., Niesman, I. R., Elias, P. M., Taupenot, L., Mahata, S. K., O'Connor, D. T., and Gallo, R. L. (2008) The neuroendocrine peptide catestatin is a cutaneous antimicrobial and induced in the skin after injury. *J. Invest. Dermatol.* 128: 1525–1534, 2008
23. Egger, M., Beer, A. G., Theurl, M., Schgoer, W., Hotter, B., Tatarczyk, T., Vasiljevic, D., Frauscher, S., Marksteiner, J., Patsch, J. R., Schratzberger, P., Djanani, A. M., Mahata, S. K., and Kirchmair, R. (2008) Monocyte migration: a novel effect and signaling pathways of catestatin. *Eur. J. Pharmacol.* **598,** 104–111
24. Mahapatra, N. R., O'Connor, D. T., Vaingankar, S. M., Hikim, A. P., Mahata, M., Ray, S., Staite, E., Wu, H., Gu, Y., Dalton, N., Kennedy, B. P., Ziegler, M. G., Ross, J., and Mahata, S. K. (2005) Hypertension from targeted ablation of chromogranin A can be rescued by the human ortholog. *J. Clin. Invest.* **115,** 1942–1952
25. Biswas, N., Rodriguez-Flores, J. L., Courel, M., Gayen, J. R., Vaingankar, S. M., Mahata, M., Torpey, J. W., Taupenot, L., O'Connor, D. T., and Mahata, S. K. (2009) Cathepsin L colocalizes with chromogranin a in chromaffin vesicles to generate active peptides. *Endocrinology* **150,** 3547–3557
26. Tsigelny, I., Mahata, S. K., Taupenot, L., Preece, N. E., Mahata, M., Khan, I., Parmer, R. J., and O'Connor, D. T. (1998) Mechanism of action of chromogranin A on catecholamine release: molecular modeling of the catestatin region reveals a beta-strand/loop/beta-strand structure secured by hydrophobic interactions and predictive of activity. *Regul. Pept.* **77,** 43–53
27. Preece, N. E., Nguyen, M., Mahata, M., Mahata, S. K., Mahapatra, N. R., Tsigelny, I., and O'Connor, D. T. (2004) Conformational preferences and activities of peptides from the catecholamine release-inhibitory (catestatin) region of chromogranin A. *Regul. Pept.* **118,** 75–87
28. Deleage, G., and Geourjon, C. (1993) An interactive graphic program for calculating the secondary structure content of proteins from circular dichroism spectrum. *Comput. Appl. Biosci.* **2,** 197–199
29. Verly, R. M., Moraes, C. M., Resende, J. M., Aisenbrey, C., Bemquemer, M. P., Pilo-Veloso, D., Valente, A. P., Alemida, F. C., and Bechinger, B. (2009) Structure and membrane interactions of the antibiotic peptide dermadistinctin k by solution and oriented ^{15}N and ^{31}P solid-state NMR spectroscopy. *Biophys. J.* **96,** 2194–2202
30. Delaglio, F., Grzesiek, S., Vuister, G. W., Zhu, G., Pfeifer, J., and Bax, A. (1995) NMRPipe: a multidimensional spectral processing system based on UNIX pipes. *J. Biomol. NMR* **6,** 277–293
31. Johnson, B. A., and Blevins, R. A. (1994) NMRVIEW: a computer program for the visualization and analysis of NMR data. *J. Biomol. NMR* **4,** 603–614
32. Hyberts, S. G., Goldberg, M. S., Havel, T. F., and Wagner, G. (1992) The solution structure of eglin c based on measurements of many NOEs and coupling constants and its comparison with X-ray structures. *Protein Sci.* **1,** 736–751
33. Schwieters, C. D., Kuszewski, J. J., Tjandra, N., and Glore, G. M. (2003) The Xplor-NIH NMR molecular structure determination package. *J. Magn. Res.* **160,** 65–73
34. Koradi, R., Billeter, M., and Wüthrich, K. (1996) MOLMOL: a program for display and analysis of macromolecular structures. *J. Mol. Graph.* **14,** 51–55
35. Bechinger, B., and Opella, S. J. (1991) Flat-coil probe for NMR spectroscopy of oriented membrane samples. *J. Magn. Reson.* **95,** 585–588
36. Hediger, S., Meier, B. H., Kurur, N. D., Bodenhausen, G., and Ernst, R. R. (1994) adiabatic cross-polarization. *Chem. Phys. Lett.* **223,** 283
37. Rance, M., and Byrd, R. A. (1983) Obtaining high-fidelity spin-1/2 powder spectra in anisotropic media: phase-cycled Hahn echo spectroscopy. *J. Magn. Res.* **52,** 221–240
38. Wenk, M., and Seelig, J. (1998) Magainin 2 amide interaction with lipid membranes: calorimetric detection of peptide binding and pore formation. *Biochemistry* **37,** 3909–3916
39. Davis, J. H., and Auger, M. (1999) Static and magic angle spinning NMR of membrane peptides and proteins. *Prog. NMR Spectroscopy* **35,** 1–84
40. Watts, A., Straus, S. K., Grage, S. L., Kamihira, M., Lam, Y. H., and Zhao, X. (2004) Membrane protein structure determination using solid-state NMR. *Methods Mol. Biol.* **278,** 403–473
41. Andronesi, O. C., Pfeifer, J. R., Al Momani, L., Ozdirekcan, S., Rijkers, D. T., Angerstein, B., Luca, S., Koert, U., Killian, J. A., and Baldus, M. (2004) Probing membrane protein orientation and structure using fast magic-angle-spinning solid-state NMR. *J. Biomol. NMR* **30,** 253–265
42. Bechinger, B., Kinder, R., Helmle, M., Vogt, T. B., Harzer, U., and Schinzel, S. (1999) Peptide structural analysis by solid-state NMR spectroscopy. *Biopolymers* **51,** 174–190
43. Thennarasu, S., Lee, D. K., Poon, A., Kawulka, K. E., Vederas, J. C., and Ramamoorthy, A. (2005) Membrane permeabilization, orientation, and antimicrobial mechanism of subtilosin A. *Chem. Phys. Lipids* **137,** 38–51
44. Ramamoorthy, A., Lee, D. K., Narasimhaswamy, T., and Nanga, R. P. (2009) Cholesterol reduces pardaxin's dynamics-a barrel-stave mechanism of membrane disruption investigated by solid-state NMR. [E-pub ahead of print] *Biochim. Biophys. Acta.* doi: 10.1016/j.bbamem.2009.08.012 **AQ: 6**
45. Salnikov, E. S., Mason, A. J., and Bechinger, B. (2009) Membrane order perturbation in the presence of antimicrobial peptides by ^{2}H solid-state NMR spectroscopy. *Biochimie (Paris)* **91,** 743
46. Mason, A. J., Martinez, A., Glaubitz, C., Danos, O., Kichler, A., and Bechinger, B. (2006) The antibiotic and DNA-transfecting peptide LAH4 selectively associates with, and disorders, anionic lipids in mixed membranes. *FASEB J.* **20,** 320–322
47. Jean-Francois, F., Desbat, B., and Dufourc, E. J. (2009) Selectivity of cateslytin for fungi: the role of acidic lipid-ergosterol membrane fluidity in antimicrobial action. *FASEB J.* **23,** 3692–3701
48. Jean-Francois, F., Castano, S., Desbat, B., Odaert, B., Roux, M., Metz-Boutigue, M. H., and Dufourc, E. J. (2008) Aggregation of cateslytin beta-sheets on negatively charged lipids promotes rigid membrane domains. A new mode of action for antimicrobial peptides? *Biochemistry* **47,** 6394–6402
49. Ramamoorthy, A. (2009) Beyond NMR spectra of antimicrobial peptides: dynamical images at atomic resolution and functional insights. *Solid State Nucl. Magn. Reson.* **35,** 201–207
50. Bechinger, B. (2009) Rationalizing the membrane interactions of cationic amphipathic antimicrobial peptides by their molecular shape. *Curr. Opin. Colloid Interface Sci.* **14,** 349–355 **AQ: 7**

51. Bechinger, B., and Sizun, C. (2003) Alignment and structural analysis of membrane polypeptides by 15N and 31P solid-state NMR spectroscopy. *Concepts Magn. Reson.* **18A,** 130–145
52. Angelone, T., Quintieri, A. M., Brar, B. K., Limchaiyawat, P. T., Tota, B., Mahata, S. K., and Cerra, M. C. (2008) The antihypertensive chromogranin a peptide catestatin acts as a novel endocrine/paracrine modulator of cardiac inotropism and lusitropism. *Endocrinology* **149,** 4780–4793
53. Jean-Francois, F., Elezgaray, J., Berson, P., Vacher, P., and Dufourc, E. J. (2008) Pore formation induced by an antimicrobial peptide: electrostatic effects. *Biophys. J.* **95,** 5748–5756
54. Henriques, S. T., Melo, M. N., and Castanho, M. A. (2006) Cell-penetrating peptides and antimicrobial peptides: how different are they? *Biochem. J.* **399,** 1–7
55. Park, C. B., Kim, H. S., and Kim, S. C. (1998) Mechanism of action of the antimicrobial peptide buforin II: buforin II kills microorganisms by penetrating the cell membrane and inhibiting cellular functions. *Biochem. Biophys. Res. Commun.* **244,** 253–257
56. Luque-Ortega, J. R., van't, H. W., Veerman, E. C., Saugar, J. M., and Rivas, L. (2008) Human antimicrobial peptide histatin 5 is a cell-penetrating peptide targeting mitochondrial ATP synthesis in Leishmania. *FASEB J.* **22,** 1817–1828
57. Alves, I. D., Goasdoue, N., Correia, I., Aubry, S., Galanth, C., Sagan, S., Lavielle, S., and Chassaing, G. (2008) Membrane interaction and perturbation mechanisms induced by two cationic cell penetrating peptides with distinct charge distribution. *Biochim. Biophys. Acta* **1780,** 948–959
58. Jung, H. J., Jeong, K. S., and Lee, D. G. (2008) Effective antibacterial action of tat (47–58) by increased uptake into bacterial cells in the presence of trypsin. *J. Microbiol. Biotechnol.* **18,** 990–996
59. Jean-Francois, F., Khemtemourian, L., Odaert, B., Castano, S., Grelard, A., Manigand, C., Bathany, K., Metz-Boutigue, M. H., and Dufourc, E. J. (2007) Variability in secondary structure of the antimicrobial peptide cateslytin in powder, solution, DPC micelles and at the air-water interface. *Eur. Biophys. J.* **36,** 1019–1027
60. Lindberg, M., and Graslund, A. (2001) The position of the cell penetrating peptide penetratin in SDS micelles determined by NMR. *FEBS Lett.* **497,** 39–44
61. Balayssac, S., Burlina, F., Convert, O., Bolbach, G., Chassaing, G., and Lequin, O. (2006) Comparison of penetratin and other homeodomain-derived cell-penetrating peptides: interaction in a membrane-mimicking environment and cellular uptake efficiency. *Biochemistry* **45,** 1408–1420
62. Magzoub, M., Eriksson, L. E., G and raslund, A. (2002) Conformational states of the cell-penetrating peptide penetratin when interacting with phospholipid vesicles: effects of surface charge and peptide concentration. *Biochim. Biophys. Acta* **1563,** 53–63
63. Herbig, M. E., Weller, K., Krauss, U., Beck-Sickinger, A. G., Merkle, H. P., and Zerbe, O. (2005) Membrane surface-associated helices promote lipid interactions and cellular uptake of human calcitonin-derived cell penetrating peptides. *Biophys. J.* **89,** 4056–4066
64. Barany-Wallje, E., Andersson, A., Graslund, A., and Maler, L. (2004) NMR solution structure and position of transportan in neutral phospholipid bicelles. *FEBS Lett.* **567,** 265–269
65. Deshayes, S., Heitz, A., Morris, M. C., Charnet, P., Divita, G., and Heitz, F. (2004) Insight into the mechanism of internalization of the cell-penetrating carrier peptide Pep-1 through conformational analysis 10. *Biochemistry* **43,** 1449–1457
66. Zasloff, M. (2002) Antimicrobial peptides of multicellular organisms. *Nature* **415,** 389–395
67. Epand, R. M., and Vogel, H. J. (1999) Diversity of antimicrobial peptides and their mechanism of action. *Biochim. Biophys. Acta* **1462,** 11–28
68. Shai, Y. (1999) Mechanism of the binding, insertion, and destabilization of phospholipid bilayer membranes by alpha-helical antimicrobial and cell non-selective lytic peptides. *Biochim. Biophys. Acta* **1462,** 55–70
69. Derossi, D., Calvet, S., Trembleau, A., Brunissen, A., Chassaing, G., and Prochiantz, A. (1996) Cell internalization of the third helix of the Antennapedia homeodomain is receptor-independent. *J. Biol. Chem.* **271,** 18188–18193
70. Ziegler, A. (2008) Thermodynamic studies and binding mechanisms of cell-penetrating peptides with lipids and glycosaminoglycans. *Adv. Drug Deliv. Rev.* **60,** 580–597
71. Ramamoorthy, A., Thennarasu, S., Tan, A., Lee, D. K., Clayberger, C., and Krensky, A. M. (2006) Cell selectivity correlates with membrane-specific interactions: a case study on the antimicrobial peptide G15 derived from granulysin. *Biochim. Biophys. Acta* **1758,** 154–163
72. Hallock, K. J., Lee, D. K., and Ramamoorthy, A. (2003) MSI-78, an Analogue of the magainin antimicrobial peptides, disrupts lipid bilayer structure via positive curvature strain. *Biophys. J.* **84,** 3052–3060
73. Lamaziere, A., Wolf, C., Lambert, O., Chassaing, G., Trugnan, G., and yala-Sanmartin, J. (2008) The homeodomain derived peptide Penetratin induces curvature of fluid membrane domains. *PLoS ONE* **3,** e1938
74. Galanth, C., Abbassi, F., Lequin, O., yala-Sanmartin, J., Ladram, A., Nicolas, P., and Amiche, M. (2009) Mechanism of antibacterial action of dermaseptin B2: interplay between helix-hinge-helix structure and membrane curvature strain. *Biochemistry* **48,** 313–327
75. Wi, S., and Kim, C. (2008) Pore structure, thinning effect, and lateral diffusive dynamics of oriented lipid membranes interacting with antimicrobial peptide protegrin-1: P-31 and H-2 solid-state NMR study. *J. Phys. Chem. B.* **112,** 11402–11414
76. Lins, L., Decaffmeyer, M., Thomas, A., and Brasseur, R. (2008) Relationships between the orientation and the structural properties of peptides and their membrane interactions. *Biochim. Biophys. Acta* **1778,** 1537–1544
77. Hansen, M., Kilk, K., and Langel, U. (2008) Predicting cell-penetrating peptides. *Adv. Drug Deliv. Rev.* **60,** 572–579
78. Tang, M., Waring, A. J., and Hong, M. (2007) Phosphate-mediated arginine insertion into lipid membranes and pore formation by a cationic membrane peptide from solid-state NMR. *J. Am. Chem. Soc.* **129,** 11438–11446
79. Bechinger, B. (1999) The structure, dynamics and orientation of antimicrobial peptides in membranes by solid-state NMR spectroscopy. *Biochim. Biophys. Acta* **1462,** 157–183
80. Hale, J. D., and Hancock, R. E. (2007) Alternative mechanisms of action of cationic antimicrobial peptides on bacteria. *Expert Rev. Anti Infect. Ther.* **5,** 951–959
81. Brogden, K. A. (2005) Antimicrobial peptides: pore formers or metabolic inhibitors in bacteria? *Nat. Rev. Microbiol.* **3,** 238–250
82. Salnikov, E. S., Friedrich, H., Li, X., Bertani, P., Reissmann, S., Hertweck, C., O'Neil, J. D., Raap, J., Bechinger, B. (2009) Structure and alignment of the membrane-associated peptaibols ampullosporin A and alamethicin by oriented ^{15}N and ^{31}P solid-state NMR spectroscopy. *Biophys. J.* **96,** 86–100

Received for publication July 23, 2009.
Accepted for publication December 17, 2009.

AUTHOR QUERIES

AUTHOR PLEASE ANSWER ALL QUERIES 1

1—INRA correctly defined as Institut National de la Recherche Agronomique in affiliation line? Pleae confirm or revise.

2—Please select a maximum of 6 key words (i.e., delete 3).

3—Please confirm or revise location (city) for supplier Fluka Please confirm or revise all instances where supplier information may be added throughout Materials and Methods.

4—BMRB correctly defined as Biological Magnetic Resonance Data Bank? Please confirm or revise.

5—Please spell out CAPES, CNPq, COFECUB, EGIDE.

6—Ref. 44: Please update if possible; otherwise, please confirm or revise doi.

7—Ref. 50: Please confirm or revise publication data.